POLITECNICO DI TORINO
Repository ISTITUZIONALE

A Test Rig for the Experimental Investigation on the Nonlinear Dynamics in the Presence of Large Contact Interfaces and Numerical Models Validation

Original
A Test Rig for the Experimental Investigation on the Nonlinear Dynamics in the Presence of Large Contact Interfaces and Numerical Models Validation / Firrone, Christian Maria; Battiato, Giuseppe. - In: JOURNAL OF VIBRATION AND ACOUSTICS. - ISSN 1048-9002. - STAMPA. - 143:3(2021), pp. 031012-1-031012-12. [10.1115/1.4048560]

Availability:
This version is available at: 11583/2850377 since: 2020-11-17T11:03:52Z

Publisher:
ASME

Published
DOI:10.1115/1.4048560

Terms of use:

This article is made available under terms and conditions as specified in the corresponding bibliographic description in the repository

Publisher copyright

(Article begins on next page)

10 April 2024

American Society of Mechanical Engineers

ASME Accepted Manuscript Repository

Institutional Repository Cover Sheet

Christian Maria (First) Firrone (Last)

ASME Paper Title: A Test Rig for the Experimental Investigation on the Nonlinear Dynamics in the Presence of Large Contact Interfaces and Numerical Models Validation

Authors: Christian Maria Firrone, Giuseppe Battiato

ASME Journal Title: Journal of Vibration and Acoustics

Volume/Issue __143/3_____ Date of Publication (VOR* Online) __October 27, 2020 _

ASME Digital Collection URL: https://asmedigitalcollection.asme.org/vibrationacoustics/article/143/3/031012/1087for-the-Experimental-Investigation-on

DOI: 10.1115/1.4048560

*VOR (version of record)

A Test Rig for the Experimental Investigation on the Non-Linear Dynamics in the Presence of Large Contact Interfaces and Numerical Models validation

Christian Maria Firrone, Giuseppe Battiato
Department of Mechanical and Aerospace Engineering, Politecnico di Torino, Corso Duca degli Abruzzi 24, 10129, Turin, Italy

Abstract

The simulation of the coupling between components modelled by Finite Elements (FE) plays an important role for the prediction of the forced response of the assembly in terms of resonant frequencies, vibration amplitudes and damping. This is particularly critical when the time-varying stress distribution must be limited for vibrating components with thin thickness coupled with large contacts. Typical examples can be found in aeronautical structures (plates, panels, bladed disk components) assembled with bolted flanges, riveted lap joints, or joints without hole discontinuities like rail-hook joints, lace wire sealings, strip dampers. In this paper a new test rig is introduced for the experimental validation of a Reduced Order Model (ROM) based on the Gram-Schmidt Interface (GSI) modes applied to a friction contact whose dimensions are not negligible with respect to the size of the substructures. In this case, classical approaches like Craig-Bampton technique might be not effective in reducing the size of the problem when many contact nodes subjected to nonlinear contact loads can not be omitted. The technique is implemented in a solution scheme in the frequency domain using penalty contact elements and the harmonic balance method. The preload on the joint is produced by permanent magnets to enhance the friction contact without introducing uncertainties due to bolting. Measurements are compared with the ROM simulations and with standard time domain integration of the full FE model. The advantage of using the GSI technique is shown in terms of time computation and accuracy of the simulation.

1 Introduction

Understanding the effects of dry friction at the interfaces of mechanical joints is a crucial task for the dynamic design of large and complex structures. Industrial applications usually involve the assembly of several components by means of either large or localized joints. The term ‘large’ is here used to define a contact interface that is distributed, i.e. its extension is not negligible with respect to the size of the structure where it is employed. In most of the applications the locking of large contact interfaces is produced by bolting (e.g., lap joints and flange joints, Fig.1a, or joints between half cases of gearbox), while for a smaller class of applications the preload at the contact interface is generated by the architecture of the system itself without extra parts (e.g., the rail-hook joint in stator vane segments of turbo-machinery in Fig.1b).
Literature about the prediction of the mechanical behavior of bolted joints and how these affect the dynamics of mechanical systems is wide, since bolt connections remain one of the most common way to assemble structures. Bolts are easily removable and can produce very large locking pressure with a limited amount of effort during the tightening operation. However, the uncertainty that characterizes the bolted joint is currently a matter of study. The validation of the mathematical models and the methodologies that predict the influence of the contact parameters, constraints, excitation level, and time influence on the dynamic response of a jointed structure requires an extensive test campaign devoted to the measurement and control of the static loads distribution determined by the initial assembly and to the vibratory response during operation (transient and forced response). The reader is invited to look at the two literature reviews [1,2] for a wide state of the art on this topic. More recent literature on the topic can be found in terms of proceedings of IMAC Congress, Session ‘Joints, Friction & Damping’ and the database of the ASME Research Committee on the Mechanics of Jointed Structures available at the link http://joints.rice.edu/ and [3].

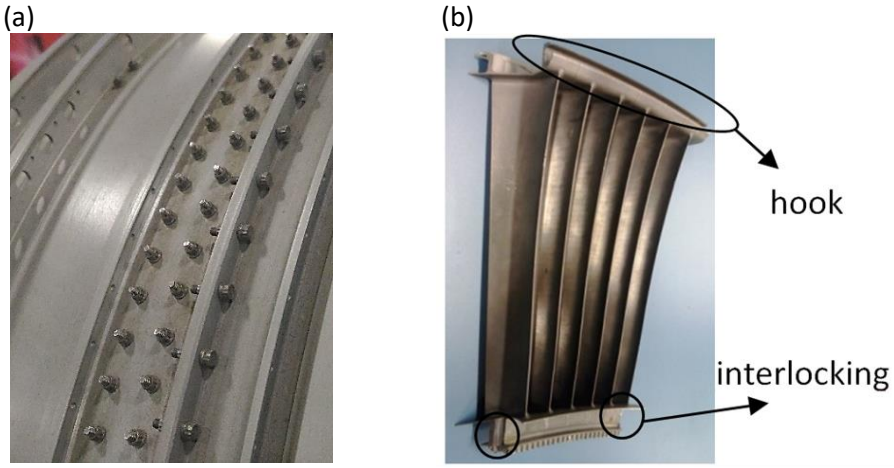

Fig.1 Example of an engine casing with lap and flange joints (a) and hook lap joints of stator vane segments (b)

The fast improvement of the computer performance in the recent past years leads industries to build FE models with highly refined meshes for structural analysis [4]. Although this practice is suitable for conventional static analyses of specific parts, modal and mode superposition harmonic analyses do not require such ultra-refined meshes and the dynamics predictability benefits from the high performance computation when it is used to extend the study to large systems made by many components. The final result is a large structural problem having multiple wide contact areas that is difficult to solve when the nonlinear dynamic behavior is considered due to the presence of large contact interfaces [5, 6]. Modeling mechanical components with FE makes in fact convenient the choice of node-to-node contact elements [7] to simulate the mutual interaction of two surfaces in contact [8-11]. However, the same choice might lead to expensive or even unfeasible numerical simulations when the nonlinear equations of motion of a huge set of contact degrees of freedom are solved in a conventional way (e.g. by using commercial FE software). In the past few years the drawback of simulating contact on regions with a high density of DoFs has been faced by employing solution strategies involving interface reduction methods [12-14]. These usually allow a modal representation of the contact interface displacements by achieving a remarkable compression on the number of nonlinear DoFs, but still preserving the interface flexibility [15]. Similar methods falling in the class of Component mode synthesis (CMS) can also be applied in multibody analysis in order to consider the nonlinear behavior of a complex mechanical assembly in the presence of large frictional joints [16,17]. Recently, the Gram-Schmidt Interface (GSI) method [18] has been proved to be well suited for dynamical problems involving large contact interfaces with a high density of DoFs [19,20].

In this paper a new, simple, test rig is presented to collect a database of nonlinear frequency response functions. The experimental test case consists of two rectangular beams held together by means of permanent magnets, choice that has been made to remove the experimental uncertainties typical for a mechanical assembly with boltings. Advantages and limitations of permanent magnets application are discussed, and a separate procedure to calibrate the magnet performance in terms of attractive force is presented.

The GSI method is then combined with a node-to-node contact elements [7] to predict the experimental nonlinear behavior of the two-beams assembly. The performance of the GSI method is then discussed with respect to that of a conventional approach, i.e. a transient nonlinear analysis performed on commercial FE software.

2 Experimental test rig

Simple structures have been already presented in literature as academic test rigs usually made by a set of beams coupled together aimed at highlighting the effect of bolted joints on the dynamics of the system [21-25]. The purpose of the test rig presented in this paper aims at reproducing the phenomenon of nonlinear damping due to friction for large contacts in order to fulfill the following requirements:

- The design of the test rig must be as simple as possible in order to clearly capture the isolated effect of friction contact in measurements and avoid high production costs.
- The assembly of the test article (i.e., the structural parts producing the friction contact and the contact pre-load) must be the simplest as well in order to emphasize the effect of the friction contact with respect to other secondary interfaces, e.g. fixtures to the ground.
- For educational and dissemination purposes, by means of the previous requirements, the complexity of the structure must be simple enough to be a transportable, academic, demonstrator of the effect of friction joints on the vibratory response of mechanical structures.

The best compromise among these requirements led to the test article shown in Fig. 2. The test article is composed of two beams having a rectangular section (400 x 30 x 3 mm) made of aluminum kept in contact together by means of cylindrical permanent magnets (diameter 17 mm, height 10 mm) that are glued on the two aluminum beams.

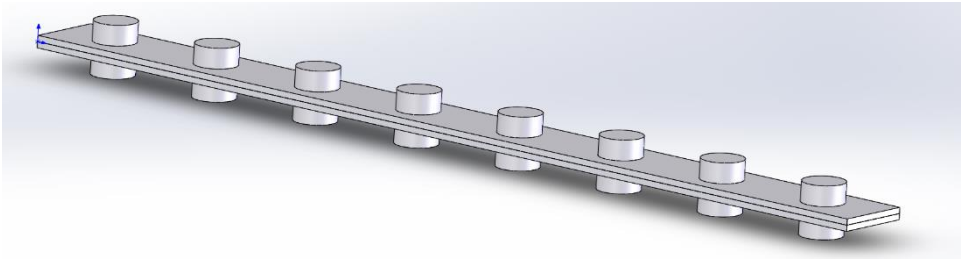

Fig.2 The test article geometry.

In this way the presence of typical locking elements like bolting are avoided in order to prevent any uncertainty in the preload generated by tightening. Moreover, frictional dissipation produced by threads and contact between head/nut and the beams' outer surfaces is avoided as well as the discontinuity on the beams' surfaces represented by holes. Damping is produced by the friction contact of the two flat surfaces only. The choice of the permanent magnets is due to the good accuracy of the level of magnetization which corresponds to a given repulsive/attractive force produced by magnets of the same class (N52) and shape. Some drawbacks can be highlighted from this design: permanent magnets can not be placed too close each other due to their lateral mutual interaction. A distance of 50 mm between their axes is used for the assembly. Then, attention must be paid for the choice of the glue between magnets and beams: due to the low bending stiffness of the beams, glued magnets can accidentally disassemble from the beams during test bench set up. Since permanent magnets are made of brittle material, an uncontrolled release of the magnets can potentially break them likely, leading to an uncontrolled failure chain due to the strong mutual attractive forces. Lastly, the contact pressure that can be achieved using permanent magnets is much lower than that possible using bolts.
The force produced by the magnets is measured by a purposely developed test rig shown in Fig. 3 which can measure both the attractive and repulsive force of two permanent magnets facing each other. Two load cells instrumented with strain gauge, Wheatstone bridges, measure the attractive force. One sliding plate moves the upper magnet along the vertical direction to measure the force at different air gaps, another sliding plate can move the lower magnet along the horizontal direction to compensate possible misalignment of the magnets. Figure 4 shows the attractive force by varying the air gap for the magnets that have been used.

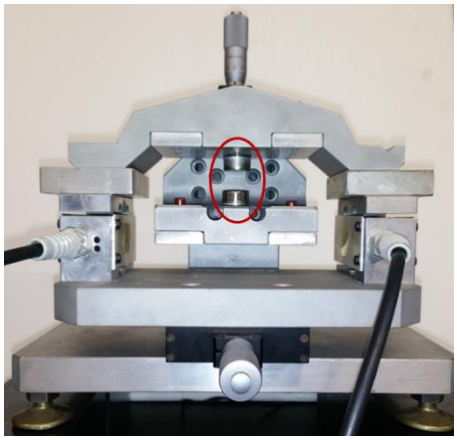

Fig.3 test rig for the static force measurement produced by a couple of permanent magnets (circled in red).

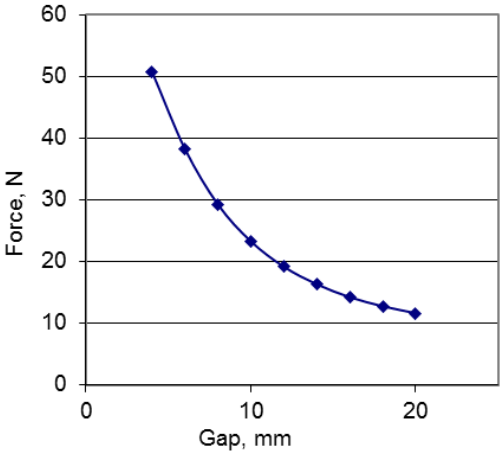

Fig.4 attractive force vs. gap diagram.

As a preliminary experimental activity, hammer tests are performed on the single beam and on the assembled structure (Fig. 5 a and b, respectively), in free-free condition, in order to identify natural frequencies, modal damping and mode shapes.

(a)

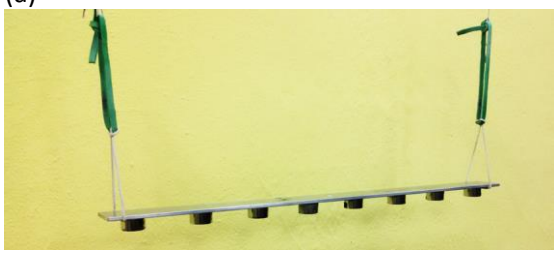

(b)

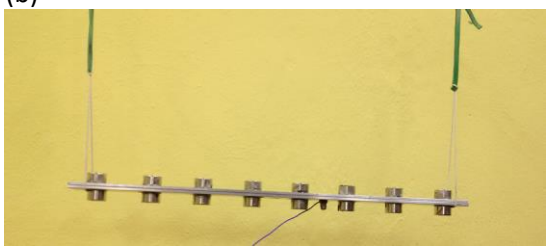

Fig.5 Hammer test, free-free condition: (a) single beam, (b) assembled system. Different rubber bands have been used to verify measurements do not depend on the constraints.

Results of the two tests are shown in Fig.6 a and b where it is possible to see the first natural frequency of the first bending mode is around 67 Hz for the single beam, and around 127 Hz for the two-beams assembly. These results will be used for the model update in the simulation phase. The half-power method is used on the single beam to identify the modal damping ratio equal to 0.006 for the first mode, this value will be used later for the simulation. Low repeatability and noisy measurements for the assembly are mainly due to two reasons: (i) the excitation of the system by hammer is difficult in the presence of permanent magnets attracting the hammer (double hit can occur and the impact point is not precise) and (ii) the damping produced by the large coupling of the two beams at the contact interface results in a very fast decay of the transient vibration.

In order to characterize the effect of friction damping on the dynamics of the system, the two-beam assembly is excited sinusoidally by means of a shaker as shown in Fig.7 (a). The shaker is used as a shaking table, the relative low weight of the assembly allows for the unusual use of the shaker without external constraints. In this way the test rig has no constraint to a fixed ground and the damping is only due to the contact surface between the beams. The effect of the small screw connecting the assembly to the shaker on the nonlinear dynamic response is considered negligible with respect to the effect of friction produced by the wide contact surface. Stepped sine testing is used to measure the Forced Response Function (FRF) in terms of inertance,

the acceleration is measured by means of an accelerometer placed close to the central constraint as shown in Fig.7 (b).

(a) (b)

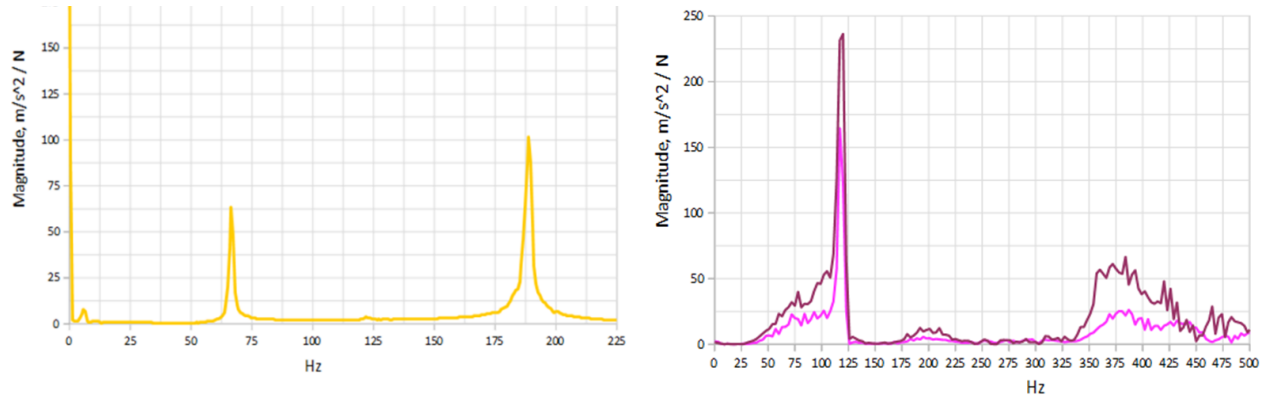

Fig.6 Experimental forced response functions, hammer test, free-free condition: (a) single beam, (b) assembled system (two different averaged measurements are shown).

Different excitation amplitudes are used (0.2 N to 10 N), the minimum value is chosen due to a limitation of the control system that does not allow for an accurate control when the excitation amplitude is too low, the maximum value is chosen to keep the structural integrity of the test article by limiting the vibration amplitudes.
Results of the test campaign are shown in Fig.8 a and b. As expected, the typical behavior of frictionally damped structures is clearly visible: as the excitation amplitude increases the vibration amplitude at resonance decreases as well as the resonant frequency.

(a) (b)

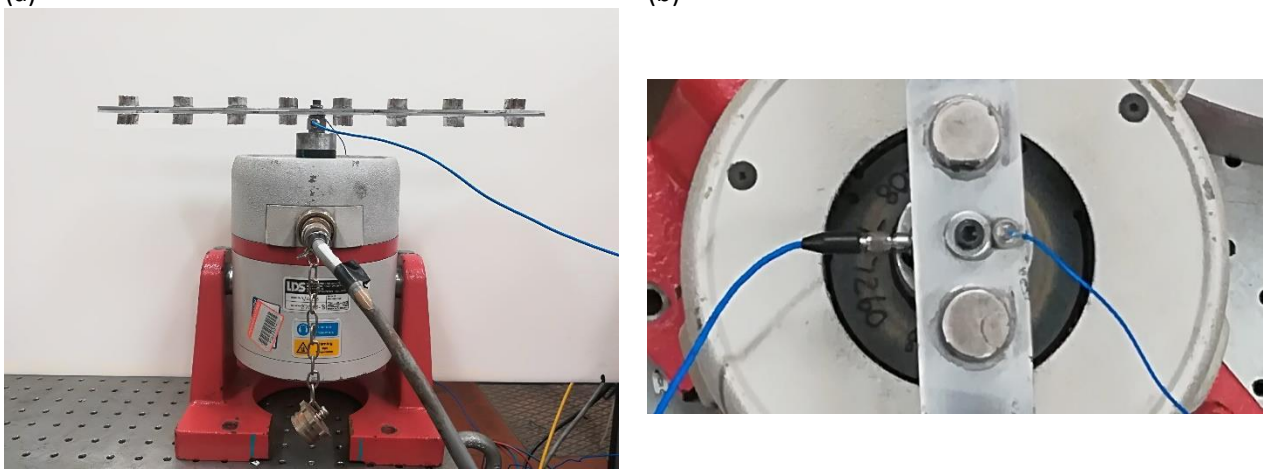

Fig.7 Excitation system (a) and measurement system (b). A load cell is placed between the assembly and the shaker for force controlled, step sine measurements.

Different trends are obtained in sweep up and sweep down tests in the region of the steep increase (sweep up) or steep decrease (sweep down) of the response for the two highest excitation amplitudes (8 N and 10 N) while the resonant amplitude is the same. This phenomenon will require further study in the future since it seems not to be related to the jump phenomenon because the response is continuous, and the force is regularly controlled. Further investigations should consider the possibility of a step sine measurement dependence on previous steps (time delay between one step and the other before sample recording,

Proportional Integral Derivative force control strategy) and the reliability of the constraint of the system with the shaker for high excitation loads (bolt loosening after several test repetitions).

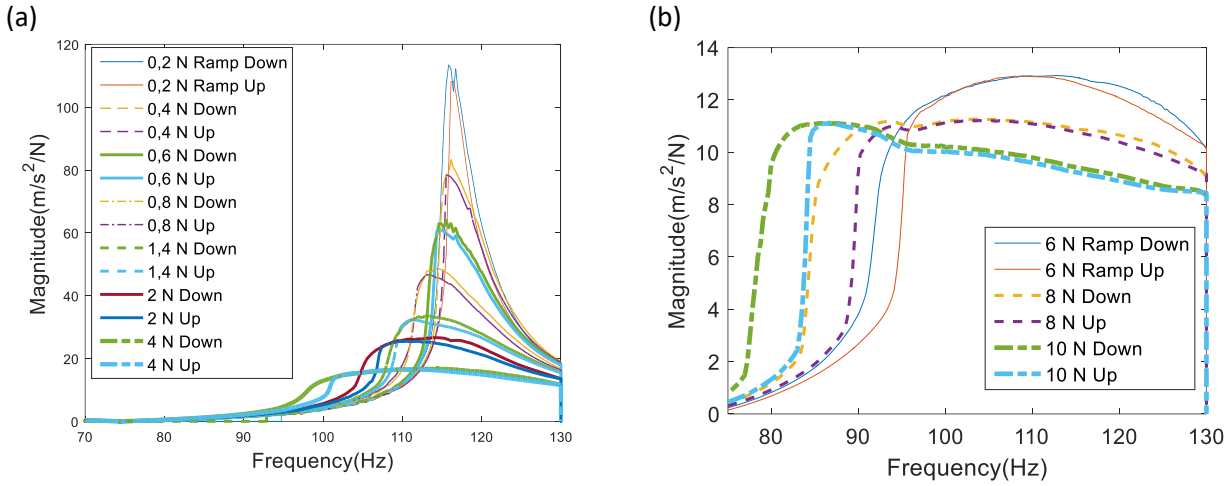

Fig.8 FRFs for 0.2 N – 4 N excitation amplitudes (a) and FRFs for 6 N - 10 N excitation amplitudes.

3 Reduction technique of large contact surfaces by means of GSI modes

The GSI method solves the problem of giving a modal representation of an arbitrary set of physical DoFs by leaving all the others in the physical space. In other words, the GSI method is used to project a specific set of physical DoFs on a modal base, usually those at the interfaces, that can be later used to solve specific problems (substructures coupling, contact simulation in the case of joint interface).

Let us assume to partition the generalized coordinate vector of a certain component as follows:

$$\boldsymbol{x} = \begin{Bmatrix} \boldsymbol{x}_m \\ \boldsymbol{q}_s \end{Bmatrix} \tag{1}$$

where:

- $\boldsymbol{x}_m$ is the vector of the n_m master DoFs, i.e. a set of physical DoFs used to perform the dynamic analysis. In this study, $\boldsymbol{x}_m$ collects a set of n_i interface DoFs $\boldsymbol{x}_i$ and possibly some others n_o physical DoFs $\boldsymbol{x}_o$ ($\boldsymbol{x}_m = [\boldsymbol{x}_i{}^T \ \boldsymbol{x}_o{}^T]^T$, so that $n_m = n_i + n_o$). Note that $\boldsymbol{x}_o$ becomes an empty vector if no other physical DoFs are required to perform the analysis except the interface ones.

- $\boldsymbol{q}_s$ is the vector of the n_s modal DoFs which exists just if a priori Component Mode Synthesis (CMS) scheme (e.g. Craig-Bampton, Rubin [26]) is applied to the FE matrices.

According to the partitioning adopted in Eqn. 1, the undamped equations of motion (EQM) of the component can be written as:

$$\begin{bmatrix} \boldsymbol{M}_{mm} & \boldsymbol{M}_{ms} \\ \boldsymbol{M}_{sm} & \boldsymbol{M}_{ss} \end{bmatrix} \begin{Bmatrix} \ddot{\boldsymbol{x}}_m \\ \ddot{\boldsymbol{q}}_s \end{Bmatrix} + \begin{bmatrix} \boldsymbol{K}_{mm} & \boldsymbol{K}_{ms} \\ \boldsymbol{K}_{sm} & \boldsymbol{K}_{ss} \end{bmatrix} \begin{Bmatrix} \boldsymbol{x}_m \\ \boldsymbol{q}_s \end{Bmatrix} = \begin{Bmatrix} \boldsymbol{f}_m \\ \boldsymbol{f}_s \end{Bmatrix} \tag{2}$$

By solving the eigenproblem defined by the partitions $\boldsymbol{K}_{mm}$ and $\boldsymbol{M}_{mm}$ a set of n_m eigenvectors called Characteristic Constraint modes is obtained [27]. These can be arranged for increasing eigenvalues as the columns of the following modal matrix:

$$\boldsymbol{\Phi}_{mm} = [\boldsymbol{\varphi}_1 \ \cdots \ \boldsymbol{\varphi}_{n_m}] \tag{3}$$

The modal matrix of Eqn. 3 would allow for a coordinate transformation of all the master DoFs. If a coordinate transformation is desired just for the subset $\boldsymbol{x}_i$, $\boldsymbol{\Phi}_{mm}$ has to be partitioned as follows:

$$\begin{Bmatrix} \boldsymbol{x}_i \\ \boldsymbol{x}_o \end{Bmatrix} = \begin{bmatrix} \boldsymbol{\Phi}_{ii} & \boldsymbol{\Phi}_{io} \\ \boldsymbol{\Phi}_{oi} & \boldsymbol{\Phi}_{oo} \end{bmatrix} \begin{Bmatrix} \boldsymbol{q}_i \\ \boldsymbol{q}_o \end{Bmatrix} \tag{4}$$

where $\boldsymbol{q}_i$ and $\boldsymbol{q}_o$ are two arbitrary set of modal coordinates with size n_i and n_o respectively. Previous studies on the GSI method proved that performing a Gram-Schmidt orthonormalization [28] on the columns of $\boldsymbol{\Phi}_{ii}$ produces a good reduction basis for the physical partition $\boldsymbol{x}_i$ [18].

The nonlinear EQM of a structure with contact interfaces can be written as:

$$\boldsymbol{M}\ddot{\boldsymbol{x}}(t) + \boldsymbol{C}\dot{\boldsymbol{x}}(t) + \boldsymbol{K}\boldsymbol{x}(t) = \boldsymbol{f}_e(t) - \boldsymbol{f}_{nl}(x, \dot{x}, t) \tag{5}$$

where $\boldsymbol{M}$, $\boldsymbol{C}$ and $\boldsymbol{K}$ are the reduced mass, damping and stiffness matrices, $\boldsymbol{x}$ is the reduced vector of DoFs, $\boldsymbol{f}_e$ and $\boldsymbol{f}_{nl}$ the corresponding vectors of the external and nonlinear contact forces. When the steady state response is of interest, it is common to solve the former EQM in the frequency domain. Due to the periodicity of $\boldsymbol{f}_e$, the displacements and nonlinear contact forces can be written according to the following Fourier series:

$$\begin{aligned} \boldsymbol{x}(t) &= \mathbb{R}\left(\sum_{h=0}^{n_h} \boldsymbol{X}^{(h)} \cdot e^{i\omega h t} \right) \\ \boldsymbol{f}_{nl}(x, \dot{x}, t) &= \mathbb{R}\left(\sum_{h=0}^{n_h} {\boldsymbol{F}_{nl}}^{(h)} \cdot e^{i\omega h t} \right) \end{aligned} \tag{6}$$

where $\boldsymbol{X}^{(h)}$ and ${\boldsymbol{F}_{nl}}^{(h)}$ are the h^{th} order Fourier coefficients of the displacements and contact forces respectively, ω is the circular frequency and n_h is the number of retained harmonics. Assuming the multi-harmonic representation of Eqn. 6, Eqn. 5 can be turned into a set of nonlinear, complex, algebraic equations:

$$\boldsymbol{D}^{(h)}\boldsymbol{X}^{(h)} = {\boldsymbol{F}_e}^{(h)} - {\boldsymbol{F}_{nl}}^{(h)}, \qquad \forall\, h = 0, \cdots, n_h \tag{7}$$

where $\boldsymbol{D}^{(h)} = \boldsymbol{K} + i\omega h\boldsymbol{C} - (\omega h)^2\boldsymbol{M}$ is the h^{th} order dynamic stiffness matrix. Note that Eqn. 7 can not be solved analytically due to its nonlinear nature but has to be solved iteratively for the multi-harmonic unknown amplitudes $\boldsymbol{X}^{(h)}$.

Let us assume to consider a structure consisting of two substructures identified by the left superscript (1) and (2). Moreover, let the number of DoFs at the contact interfaces be the same, i.e. $n_i^{(1)} = n_i^{(2)} = n_i$. Under these assumptions, the global mass and stiffness matrices and the vectors of Eqn. 7 can be expressed as:

$$\boldsymbol{M} = \begin{bmatrix} {}^{(1)}\boldsymbol{M}_{ii} & {}^{(1)}\boldsymbol{M}_{io} & \boldsymbol{0} & \boldsymbol{0} \\ {}^{(1)}\boldsymbol{M}_{oi} & {}^{(1)}\boldsymbol{M}_{oo} & \boldsymbol{0} & \boldsymbol{0} \\ \boldsymbol{0} & \boldsymbol{0} & {}^{(2)}\boldsymbol{M}_{ii} & {}^{(2)}\boldsymbol{M}_{io} \\ \boldsymbol{0} & \boldsymbol{0} & {}^{(2)}\boldsymbol{M}_{oi} & {}^{(2)}\boldsymbol{M}_{oo} \end{bmatrix} \quad \boldsymbol{K} = \begin{bmatrix} {}^{(1)}\boldsymbol{K}_{ii} & {}^{(1)}\boldsymbol{K}_{io} & \boldsymbol{0} & \boldsymbol{0} \\ {}^{(1)}\boldsymbol{K}_{oi} & {}^{(1)}\boldsymbol{K}_{oo} & \boldsymbol{0} & \boldsymbol{0} \\ \boldsymbol{0} & \boldsymbol{0} & {}^{(2)}\boldsymbol{K}_{ii} & {}^{(2)}\boldsymbol{K}_{io} \\ \boldsymbol{0} & \boldsymbol{0} & {}^{(2)}\boldsymbol{K}_{oi} & {}^{(2)}\boldsymbol{K}_{oo} \end{bmatrix}$$

$$\boldsymbol{X}^{(h)} = \begin{Bmatrix} {}^{(1)}\boldsymbol{X}_i{}^{(h)} \\ {}^{(1)}\boldsymbol{X}_o{}^{(h)} \\ {}^{(2)}\boldsymbol{X}_i{}^{(h)} \\ {}^{(2)}\boldsymbol{X}_o{}^{(h)} \end{Bmatrix} \qquad \boldsymbol{F}_e{}^{(h)} = \begin{Bmatrix} 0 \\ {}^{(1)}\boldsymbol{F}_{e,o}{}^{(h)} \\ 0 \\ {}^{(2)}\boldsymbol{F}_{e,o}{}^{(h)} \end{Bmatrix} \qquad \boldsymbol{F}_{nl}{}^{(h)} = \begin{Bmatrix} {}^{(1)}\boldsymbol{F}_{nl,i}{}^{(h)} \\ 0 \\ {}^{(2)}\boldsymbol{F}_{nl,i}{}^{(h)} \\ 0 \end{Bmatrix} \tag{8}$$

Since $\boldsymbol{F}_{nl}{}^{(h)}$ only depends on the relative displacements at the contact interface, the number of nonlinear algebraic equations corresponding to the interface DoFs can be halved by employing the coordinate transformation from absolute to relative displacements at the contact interface. By defining the relative displacement vector at the contact interface as:

$${}^{(r)}\boldsymbol{X}_i{}^{(h)} = {}^{(1)}\boldsymbol{X}_i{}^{(h)} - {}^{(2)}\boldsymbol{X}_i{}^{(h)} \tag{9}$$

the vector $\boldsymbol{X}^{(h)}$ becomes:

$$\boldsymbol{X}^{(h)} = \begin{Bmatrix} {}^{(1)}\boldsymbol{X}_i{}^{(h)} \\ {}^{(1)}\boldsymbol{X}_o{}^{(h)} \\ {}^{(2)}\boldsymbol{X}_i{}^{(h)} \\ {}^{(2)}\boldsymbol{X}_o{}^{(h)} \end{Bmatrix} = \begin{bmatrix} \boldsymbol{I} & \boldsymbol{0} & \boldsymbol{I} & \boldsymbol{0} \\ \boldsymbol{0} & \boldsymbol{I} & \boldsymbol{0} & \boldsymbol{0} \\ \boldsymbol{0} & \boldsymbol{0} & \boldsymbol{I} & \boldsymbol{0} \\ \boldsymbol{0} & \boldsymbol{0} & \boldsymbol{0} & \boldsymbol{I} \end{bmatrix} \begin{Bmatrix} {}^{(r)}\boldsymbol{X}_i{}^{(h)} \\ {}^{(1)}\boldsymbol{X}_o{}^{(h)} \\ {}^{(2)}\boldsymbol{X}_i{}^{(h)} \\ {}^{(2)}\boldsymbol{X}_o{}^{(h)} \end{Bmatrix} = \boldsymbol{R}\boldsymbol{X}_r{}^{(h)} \tag{10}$$

where $\boldsymbol{R}$ is the coordinate transformation matrix. By projecting Eqn. 7 onto the space spanned by the columns of $\boldsymbol{R}$, the following system of equations is obtained:

$$\boldsymbol{R}^T\boldsymbol{D}^{(h)}\boldsymbol{R}\boldsymbol{X}_r{}^{(h)} = \boldsymbol{R}^T\boldsymbol{F}_e{}^{(h)} - \boldsymbol{R}^T\boldsymbol{F}_{nl}{}^{(h)}, \qquad \forall\, h = 0, \cdots, n_h \tag{11}$$

From Eqn. 11 it can be realized that $\boldsymbol{F}_e{}^{(h)}$ remain unchanged despite the pre-multiplication by $\boldsymbol{R}^T$, while $\boldsymbol{F}_{nl}{}^{(h)}$ becomes:

$$\boldsymbol{F}_{nl,r}{}^{(h)} = \boldsymbol{R}^T\boldsymbol{F}_{nl}{}^{(h)} = \begin{bmatrix} \boldsymbol{I} & \boldsymbol{0} & \boldsymbol{0} & \boldsymbol{0} \\ \boldsymbol{0} & \boldsymbol{I} & \boldsymbol{0} & \boldsymbol{0} \\ \boldsymbol{I} & \boldsymbol{0} & \boldsymbol{I} & \boldsymbol{0} \\ \boldsymbol{0} & \boldsymbol{0} & \boldsymbol{0} & \boldsymbol{I} \end{bmatrix} \begin{Bmatrix} {}^{(1)}\boldsymbol{F}_{nl,i}{}^{(h)} \\ \boldsymbol{0} \\ {}^{(2)}\boldsymbol{F}_{nl,i}{}^{(h)} \\ \boldsymbol{0} \end{Bmatrix} = \begin{Bmatrix} {}^{(1)}\boldsymbol{F}_{nl,i}{}^{(h)} \\ \boldsymbol{0} \\ {}^{(1)}\boldsymbol{F}_{nl,i}{}^{(h)} + {}^{(2)}\boldsymbol{F}_{nl,i}{}^{(h)} \\ \boldsymbol{0} \end{Bmatrix} = \begin{Bmatrix} {}^{(1)}\boldsymbol{F}_{nl,i}{}^{(h)} \\ \boldsymbol{0} \\ \boldsymbol{0} \end{Bmatrix} \tag{12}$$

meaning that the Fourier coefficients of the contact forces ${}^{(1)}\boldsymbol{F}_{nl,i}{}^{(h)}$ and ${}^{(2)}\boldsymbol{F}_{nl,i}{}^{(h)}$ are equal in amplitude but opposite in sign. In this way the number of nonlinear EQM finally decreases from $2 \times n_i$ to n_i.

Due to the large extension of the contact interfaces, a further reduction of the DoFs can be achieved by employing the GSI method. If $\boldsymbol{\Phi}_{iw}$ is a $n_i \times n_w$ reduced basis of GSI interface modes with $n_w \ll n_i$, the vector $\boldsymbol{X}_r{}^{(h)}$ can be approximated as:

$$\begin{Bmatrix} {}^{(r)}\boldsymbol{X}_i{}^{(h)} \\ {}^{(1)}\boldsymbol{X}_o{}^{(h)} \\ {}^{(2)}\boldsymbol{X}_i{}^{(h)} \\ {}^{(2)}\boldsymbol{X}_o{}^{(h)} \end{Bmatrix} = \begin{bmatrix} \boldsymbol{\Phi}_{iw} & \boldsymbol{0} & \boldsymbol{0} & \boldsymbol{0} \\ \boldsymbol{0} & \boldsymbol{I} & \boldsymbol{0} & \boldsymbol{0} \\ \boldsymbol{0} & \boldsymbol{0} & \boldsymbol{I} & \boldsymbol{0} \\ \boldsymbol{0} & \boldsymbol{0} & \boldsymbol{0} & \boldsymbol{I} \end{bmatrix} \begin{Bmatrix} {}^{(r)}\boldsymbol{Q}_w{}^{(h)} \\ {}^{(1)}\boldsymbol{X}_o{}^{(h)} \\ {}^{(2)}\boldsymbol{X}_i{}^{(h)} \\ {}^{(2)}\boldsymbol{X}_o{}^{(h)} \end{Bmatrix} = \boldsymbol{G}\boldsymbol{X}_{r,GSI}{}^{(h)} \tag{13}$$

where ${}^{(r)}\boldsymbol{Q}_w{}^{(h)}$ is the vector of the complex amplitudes corresponding to the GSI modal coordinates ${}^{(r)}\boldsymbol{q}_w$. By projecting each Eqn. 11 onto the space spanned by the columns of $\boldsymbol{G}$, the following reduced order model is obtained:

$$\boldsymbol{G}^T\boldsymbol{R}^T\boldsymbol{D}^{(h)}\boldsymbol{R}\boldsymbol{G}\boldsymbol{X}_{r,GSI}{}^{(h)} = \boldsymbol{G}^T\boldsymbol{R}^T\boldsymbol{F}_e{}^{(h)} - \boldsymbol{G}^T\boldsymbol{R}^T\boldsymbol{F}_{nl}{}^{(h)}, \qquad \forall\, h = 0, \cdots, n_h \tag{14}$$

with

$$\boldsymbol{G}^T\boldsymbol{R}^T\boldsymbol{F}_{nl}{}^{(h)} = \begin{Bmatrix} \boldsymbol{\Phi}_{iw}^T{}^{(1)}\boldsymbol{F}_{nl,i}{}^{(h)} \\ 0 \\ 0 \\ 0 \end{Bmatrix} \tag{15}$$

where the term $\boldsymbol{\Phi}_{iw}^T{}^{(1)}\boldsymbol{F}_{nl,i}{}^{(h)}$ represents the vector of modal contact forces in the GSI space. Although the complex amplitudes ${}^{(1)}\boldsymbol{F}_{nl,i}{}^{(h)}$ are always computed in the space of the physical DoFs, these are introduced into the EQM in a reduced form. This procedure allows a faster solution of the nonlinear partition of Eqn. 14, that otherwise would be computationally expensive as in the case of Eqn. 11.

The strategy used to build the reduced basis of $\boldsymbol{\Phi}_{iw}$ is later discussed since it strictly depends on the physics behind the contact phenomena at the interfaces between the substructures.

4 Application of the methodology and comparisons with measurements

Simulations are performed with the FE model of the same system presented in the previous section for numerical/experimental comparison purposes. First, a mesh convergence study is performed. Since time domain analysis is one of the activities planned for the simulation of the effect of friction damping on the dynamics of the two beam assembly, a compromise between number of elements and mesh convergence is found. The final FE model is discretized with 20-node hexahedral elements with the following material properties: aluminum Young's modulus E = 64.72 GPa, magnets Young's modulus E = 6.472 GPa, aluminum density 2800 kg/m^3, magnets density 8951 kg/m^3, Poisson's ratio 0.33. The single beam FE model has 52463 elements and 89140 nodes, while the assembled system with merged nodes at the contact interface consists of 104926 elements and 172130 nodes. The total number of contact nodes is equal to 2080, which corresponds to 6240 DoFs. A model update is performed by using hammer tests previously carried out on the single beam in free-free condition. Table 1 shows the relative percentage error obtained in the two configurations. It is possible to see that the comparison for the full assembly shows a higher positive percentage error due to the partially separated contact surfaces in the physical assembly.

Table 1

	Natural frequency FEM	Natural frequency exp.	% error wrt experiments
Single beam	68.2 Hz	66.7 Hz	2.2 %
Assembled system	126.5 Hz	117 Hz	8.1 %

In order to perform the nonlinear calculation in the presence of friction damping, a layer of uniformly distributed contact elements is defined. The choice of placing contact elements through all the nominal contact area comes from the following considerations:

1) for a general application where also gaskets are inserted in a bolted flange, contact elements must be used through all the surface since local separations are, in this specific case, not expected to prevent leakage;

2) From a practical point of view, it is easier to uniformly distribute contact elements over the contact surface rather than select potential contact areas;
3) An optical topography measurement of the contact surfaces is performed based on focus variation. Three regions (30 mm x 4 mm wide) covering an area which is partly directly subjected to the pressure of the magnet (under the circular area of the magnet) are selected (Fig.9, grey dashed rectangle). Nine paths, each 4-millimeter long, are selected inside the two areas (red lines of Fig.9) to measure the roughness and the actual percentage of contact surface according to EN ISO 4287/4288. The average roughness is 1.14 µm (0.13 standard deviation) corresponding to a fine surface finishing. A typical Firestone-Abbott curve obtained by data processing is shown in Fig.10. The depth corresponding to *Svk* can be interpreted as the valley depth below the core material while the percentage of area defined by *Rmr,2* indicates the area that will carry the load. The average value of *Rmr,2* is 91%. 3D scan can be used to define specific contact models taking into account meso- and micro-scale properties of the surface as shown in [29] where tractions in the normal and tangential directions and corresponding stiffness are based on the equivalence of the asperities to the Hertzian contact. In this study, the morphology evaluation only indicated a pretty flat surface, potentially subjected to an almost complete contact under the preload. Furthermore, it showed the same properties both in the region directly involved in the contact and the rest of the area, unmodified by the tests due to the low amount of the preload and the low number of cycles produced during step sine tests.

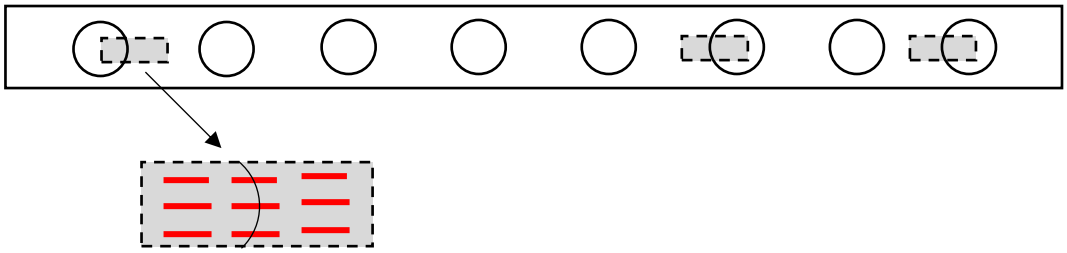

Fig.9 Regions involved in the topography measurement (grey areas) and paths for the roughness measurement (red segments).

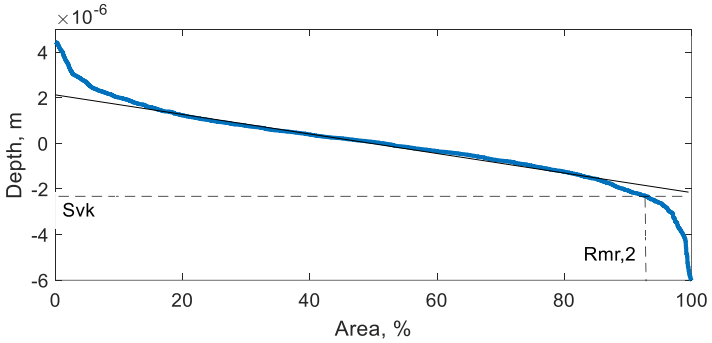

Fig.10 Example of the Firestone-Abbott curve measured for one segment measurement.

4.1 Numerical simulation of the full FE model by Time Domain Analysis (TDA)

Before applying the methodology introduced in this paper, a preliminary simulation of the forced response in the time domain by integrating the equation of motion is presented. Time Domain Analysis (TDA) is a standard approach that is possible to develop in a FE commercial software to simulate the nonlinear effects due to friction contacts during dynamic excitation. FE element commercial software offer simplified procedures and specific tools to deal with contact problems in order to help the user to correctly set up the

boundary conditions of the problem (pre-processing) and to monitor the outcomes of the simulation (post-processing). A layer of surface-to-surface CONTA174-TARGE170 elements are used in Ansys to benefit of the specific tools available in the software dealing with contact problems. First, a static nonlinear analysis is performed in Ansys to calculate the initial preload on the contact surface produced by the application of the eight couples of permanent magnets. The FE model used to perform this analysis is that shown in Fig.15, where the beams and magnets are meshed by using brick elements with the previously declared material properties. Lagrange multiplier formulation is applied on the contact surfaces. A value of 38 N compressive force is used for each couple of magnets as suggested by the measured map shown in Fig.3 (6 mm air gap) by dividing it by the number of nodes of the top circular area of the magnet and applying it in the same area as a set of equivalent nodal forces. It is possible to see from Fig.11 that the preload is far from a uniform distribution. In particular, a partially separated, receding, contact is clearly visible. As defined in [30], a receding contact is a contact "where the application of a normal load causes a reduction in the size of the contact". In this case, the large compliance of the beams induces separation in the contact regions that are not directly pressed by the permanent magnets.

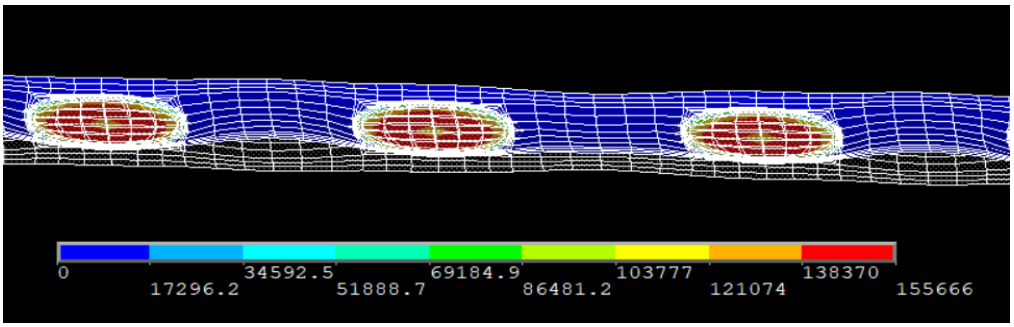

Fig.11 Contact pressure distribution and deformed shape at the contact showing the receding contact (values are in Pascal).

Augmented Lagrange formulation is then used to solve the transient response contact problem since the pure Lagrange multiplier did not allow to achieve a converged solution. Although the Augmented Lagrange formulation allows for a more robust convergence of the solution, it requires the definition of several contact parameters, the most important among them are the penalty stiffness along the normal and tangential direction (respectively FKN and FKT coefficients). These values can be defined as absolute or relative values with respect to the core material properties, a sensitivity study was performed and shown in Fig.12 by applying a harmonic displacement in a group of nodes located in correspondence of the screw connecting the system to the shaker. The time response of a node located on the free end of the upper beam is plotted when FKN (upper plot) and FKT (lower plot) are varied. It is possible to see the difference of the amplitude of the steady solution varies less than 10%.

A series of transient simulations are performed by exciting the system with a harmonic force in correspondence of the stinger that is connected to the beams for several excitation frequencies in order to reconstruct the forced responses. A damping factor proportional to the stiffness matrix is defined. Starting from the definition of the modal damping ratio associated to the *r-th* mode: $\zeta_r = \alpha \frac{1}{2\omega_r} + \beta \frac{\omega_r}{2}$, α is arbitrarily set to *0* and β is calculated since ζ_1 and ω_1 are known for the first mode. The choice for the friction coefficient is subjected to a sensitivity analysis (0.6 , 0.7 , 0.8) and a value of 0.7 is used for the results shown in this section. The same value will be used for the calculation in the frequency domain.

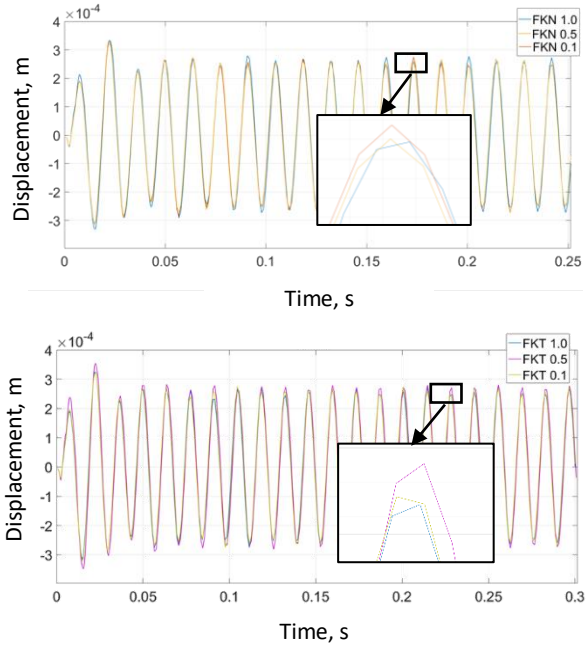

Fig. 12 sensitivity study of FKN and FKT penalty stiffness

The order of magnitude of the time required for a single simulation at a given excitation frequency is 10 hours. The comparison with the experimental measurements is shown in Fig.13 a) and b) for two excitation force amplitudes, 0.6N and 2N. The continuous line of the TDA plots connects dot markers that represent the steady state response amplitudes that were actually calculated. Although the simulated peak amplitudes agree well with the measured ones the resonant frequency is not predicted correctly. Further investigation on the effect of the number of contact elements, mesh refinement, different contact formulation, and variation of the contact parameters is suggested to understand the reason for this difference. The simulations presented here are not meant for a direct comparison with the simulations obtained in the frequency domain using the Reduced Order Model (ROM) described in the previous section. It only proves that the simulation of a wide friction contact with standard approaches allowed by FE software may be computationally prohibitive and not fully satisfactory in terms of predictability of the forced response.

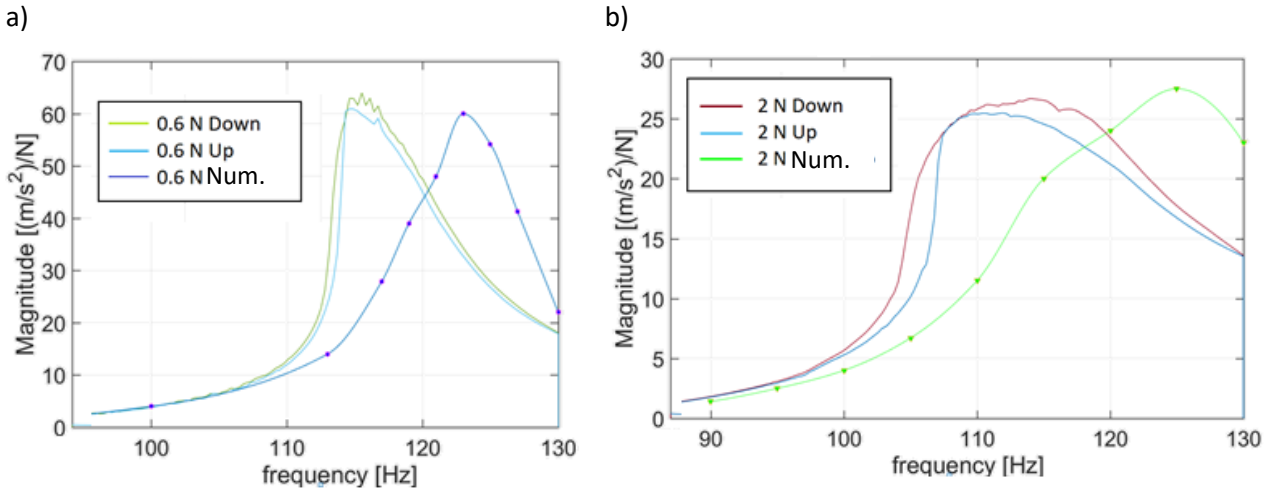

Fig.13 Comparison between TDA and experimental measurements: a) 0.6N and b) 2N excitation amplitudes.

4.2 Numerical simulation with reduced order modelling by Frequency Domain Analysis (FDA)

The methodology introduced in this paper is now applied. Different steps of reduction are employed in order to achieve a significant discount on the expected computational costs. First, by looking at Fig.14 and 15, it can be noted the presence of a symmetry plane for the test case geometry and the mode shape under consideration.

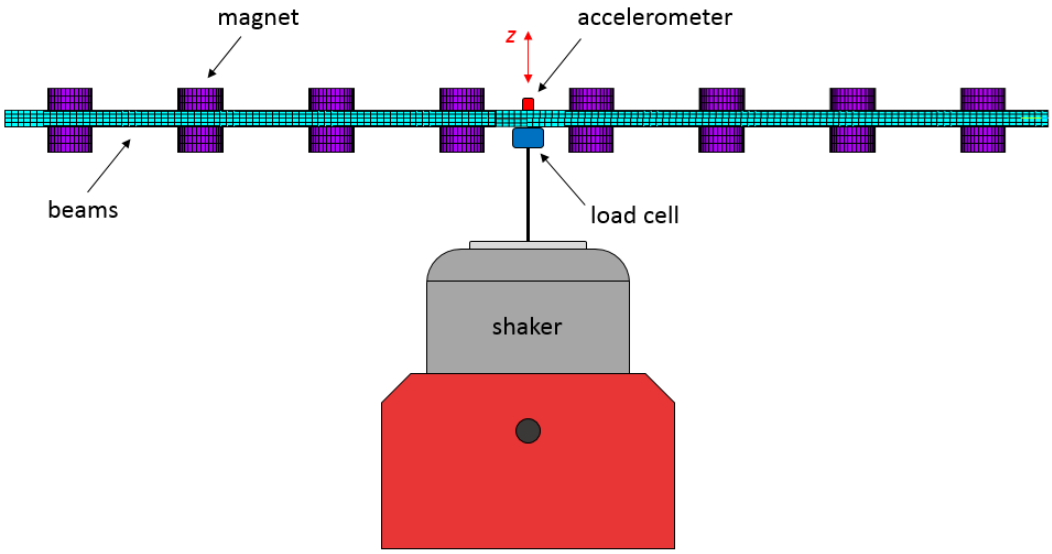

Fig.14 Schematic view of the experimental test rig.

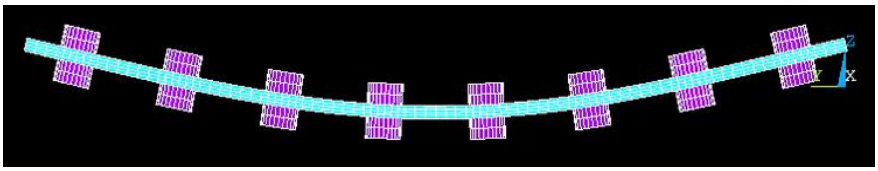

Fig.15 First mode shape of the assembly according to a modal analysis performed with Ansys

By exploiting the mentioned symmetry, it can be easily realized that just half of the FE model is sufficient to perform the same dynamic analyses without losing accuracy in the results. In particular, the part of the FE model retained for the dynamic analyses goes from the location where the beams are excited by the shaker to one of their free ends. In order to satisfy the kinematic conditions required by the mode shape of Figure 15, the removed part is replaced with a set of supports reacting along the y-axis (axis of the beams), applied at all the nodes belonging to the symmetry plane (Figure 16). The result of this process is exactly a 50% decrease on the number of nonlinear DoFs (i.e. from 6240 to 3120).

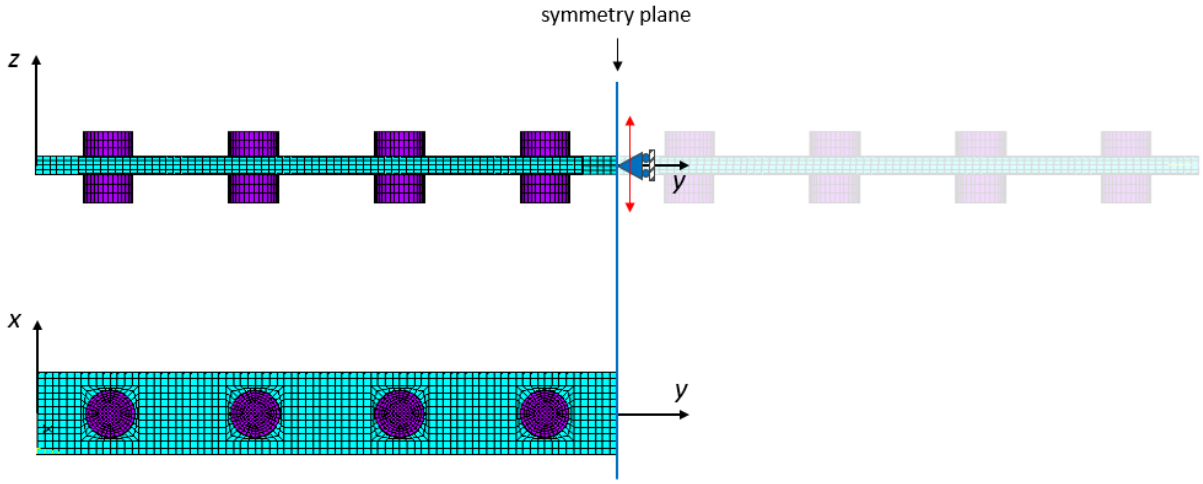

Fig.16 Symmetry plane used for the simulation

Second, the two half-beams are reduced according to the CMS-Craig Bampton technique by using a standard procedure in Ansys APDL. For each half beam the retained master DoFs are those highlighted in Fig.17, i.e. the set of 351 active DoFs lying on the symmetry plane that are used to apply the shaker excitation and 3120 DoFs at the contact interface.

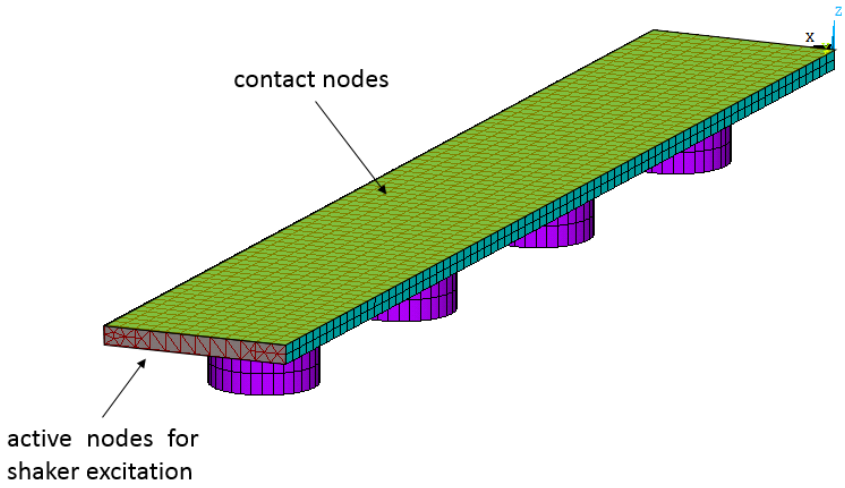

Fig.17 Set of master nodes retained for CMS-Craig Bampton reduction.

Third, the Craig-Bampton stiffness and mass matrices are imported in Matlab, constraints on the symmetry plane are included in order to prevent rigid body motion along the Y direction. A further reduction of the interface DoFs can be achieved by the GSI method and the nonlinear calculations in the frequency domain performed with the Harmonic Balance Method.
Before showing the applications of the GSI method, some considerations on the contact state at the interface are needed in order to proceed with the choice of the GSI modal basis.

4.2.1 GSI modal basis selection

Depending on the nature of the external excitation, preload and contact parameters, the system's response usually follows the typical trend of the slip-stick nonlinear phenomenon (Figure 18).

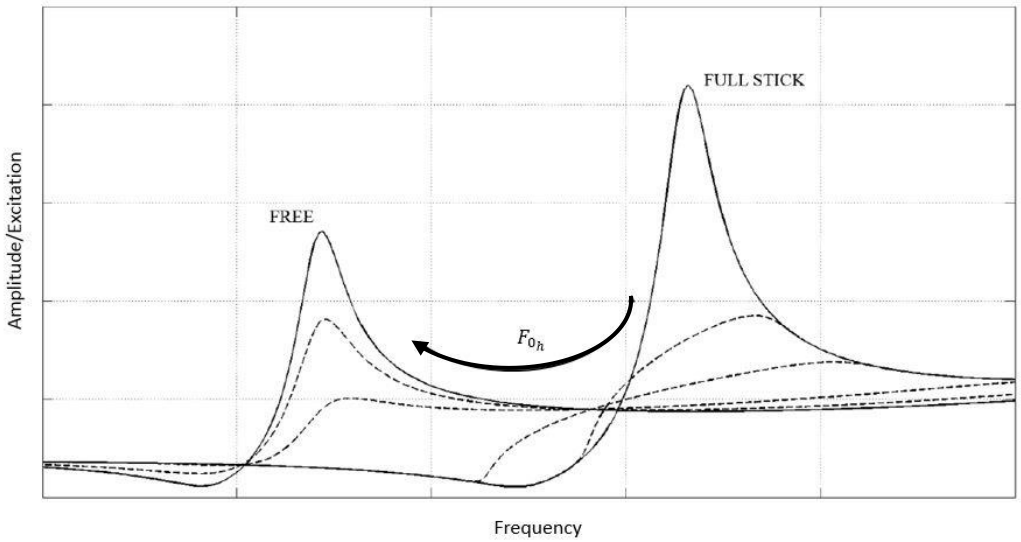

Fig.18 Stick-slip phenomenon in the frequency domain: for a fixed value of the normal preload an increase of the excitation amplitude F_0 shifts the resonance towards the free response.

For a fixed value of the static preload, an increase of the external load has the effect of shifting the resonant frequency towards lower values, moving from the full-stick condition (i.e. no sliding occurs during the whole vibration cycle) to the free condition (i.e. when contact occurs during the whole vibration cycle). Similarly, for a fixed value of the external load, the system response moves from the full-stick to the free condition when the static preload decreases. It is also quite crucial understanding the nature of the structure's mode shapes for these two extreme conditions: in the free case, the mode shapes coincide to those of the isolated beam, while in the fully stuck case the mode shapes are those of the coupled structure.
According to the previous observations, the contact DoFs might be approximated with a basis of GSI modes that has to well describe the interface motion for both the free and full-stick configurations. In [19-20] authors have found that a reliable approximation of the displacement field at the contact interface can be achieved by combining the GSI modes obtained for non-contacting (i.e. free, Fig.19 left) and stick conditions. In particular, the mentioned GSI basis is created by applying the mathematical procedure defining $\boldsymbol{\Phi}_{iw}$ to two sets of linear matrices:

- the free matrices $\boldsymbol{M}_{r,fr}$ and $\boldsymbol{K}_{r,fr}$ (Fig. 14 left) obtained by just applying the coordinate transformation of Eqn. 10 to the mass and stiffness matrix of Eqn. 8;

- the full stick matrices $\boldsymbol{M}_{r,fs}$ and $\boldsymbol{K}_{r,fs}$ defined as:

$$\boldsymbol{M}_{r,fs} = \boldsymbol{M}_{r,fr} \qquad \begin{cases} \boldsymbol{K}_{fs} = \boldsymbol{K} + \boldsymbol{K}_{link} \\ \boldsymbol{K}_{r,fs} = \boldsymbol{R}^T \boldsymbol{K}_{fs} \boldsymbol{R} \end{cases} \tag{16}$$

where $\boldsymbol{K}_{link}$ performs the assembly of the matrices ${}^{(1)}\boldsymbol{K}$ and ${}^{(2)}\boldsymbol{K}$ by means of a set of node-to-node springs having the same stiffness values that are used for the contact elements (Fig. 19 right). In this way, two bases of non-GSI modes are obtained ($\boldsymbol{\Phi}_{ii}$ of Eqn. 4), i.e. $\boldsymbol{\Phi}_{ii}^{fr}$ and $\boldsymbol{\Phi}_{ii}^{fs}$ from the free and full-stick models respectively. The strategy adopted to accomplish the mentioned task is based on the definition of a reduction basis with $n_w \ll n_i$ modes kept from the bases $\boldsymbol{\Phi}_{ii}^{fr}$ and $\boldsymbol{\Phi}_{ii}^{fs}$:

$$\boldsymbol{\Phi}_{iw} = \left[\boldsymbol{\Phi}_{iw_{fr}}^{fr} \quad \boldsymbol{\Phi}_{iw_{fs}}^{fs} \right] \tag{17}$$

where the subscripts w_{fr} and w_{fs} denote the number of modes (even unequal) retained from each basis, i.e. $n_{w_{fr}}$ and $n_{w_{fs}}$ for $\boldsymbol{\Phi}_{iw_{fr}}^{fr}$ and $\boldsymbol{\Phi}_{iw_{fs}}^{fs}$ respectively. The final GSI reduction basis is therefore obtained by performing a Gram-Schmidt orthonormalization on the non-GSI basis $\boldsymbol{\Phi}_{iw}$, which ensures linear independency for all the collected modes. In [19] it has been also proved that $\boldsymbol{\Phi}_{iw}$ can properly represent the kinematics at the contact interface in the case of local separation which leads to the jump phenomenon in the forced response.
A convergence analysis similar to that carried out in [19] assessed that 50 is the minimum number of GSI modes for a satisfactorily approximation of the kinematics at the contact interface between the beams. 25 GSI modes were obtained assuming a free boundary condition at the contact interface, while the remaining 25 correspond to the full-stick condition.

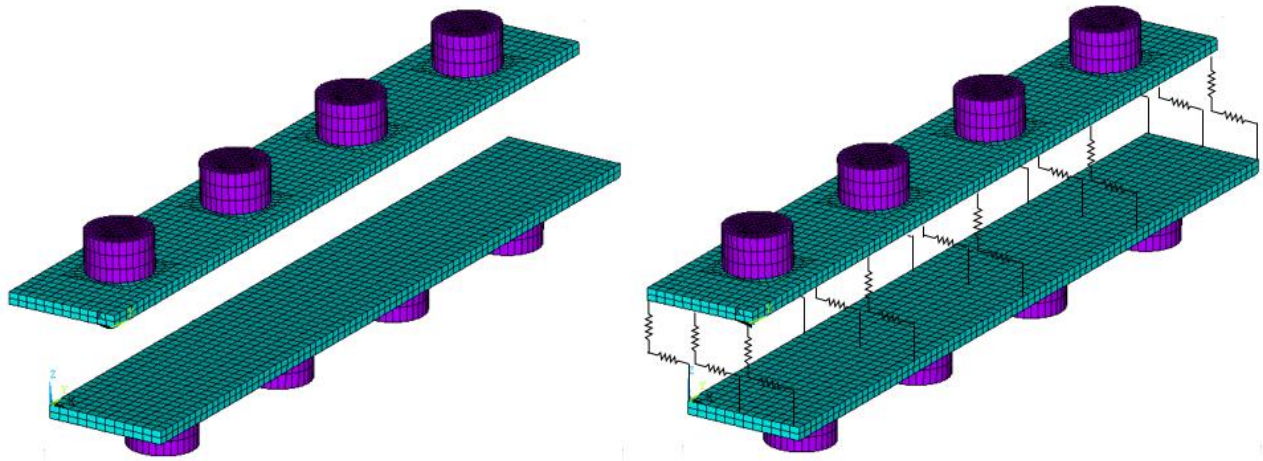

Fig.19 Coupling is absent in the free condition (left figure) while contact stiffnesses link linearly the two beams in the full stick condition (right figure, links are also applied along the y direction but are not shown here for clarity).

4.2.2 Nonlinear calculation and comparison with experimental measurements

Two strategies can be implemented to take into account the friction effects at the surface: node-to-node contact elements like Jenkins contact elements used all over the surface as in [31], or purposely developed contact models (taking into account the particular kinematics of the assembly or the nature of the joint) in order to reduce the level of complexity in the simulation of the friction nonlinearity, see for instance [6], and [32] where the whole joint approach is presented. In this paper, the first strategy is used. The contact model is a node-to-node 2D contact element allowing for variable normal load and 1D tangential slipping [7]. The contact model's parameters are represented by the tangential and normal contact stiffnesses, k_t and k_n respectively, the friction coefficient μ and the normal preload f_0. Two approaches for the definition of the contact stiffness can be used, they can be directly experimentally identified [33] or the values can be retrieved according to a global tuning with the dynamic response of the vibrating system. In this paper the second approach is used. The tangential and normal contact stiffness are here defined as $k_t = k_n$ and their value is chosen in order to obtain the value of the first resonant frequency that is experimentally measured by means of the hammer test for very low excitation amplitudes (Fig. 6b, 117 Hz), a friction coefficient of 0.7 as in TDA is used in this analysis.
Two contact elements are placed orthogonally for the same couple of mating nodes in order to take into account 2D planar motion. However, bending vibrations along the length of the beams is expected due to the type of excitation and the frequency range of the tests. The analytical Jacobian including the partial derivatives of the contact forces with respect to the relative displacements is implemented [8]. The structural

damping matrix is defined, like in the TDA, as proportional to the stiffness matrix and the identified modal damping ratio for the first mode is used.
Simulations are performed using the same excitation amplitudes that are used in the test campaign. The pressure distribution shown in Fig.11 is imported in the contact model as equivalent nodal forces (one per contact pair) for the dynamic nonlinear calculation of the FRF. In the region where separation occurs a negative value of preload equal to the gap multiplied by the normal contact stiffness is introduced. Nonlinear dynamic calculations are performed with a number of harmonics equal to 3. The order of magnitude of time requested by the presented methodology to calculate a single FRF is less than 10 minutes instead of 10 hours needed for the TDA, depending on the number of contact elements that are actually in a slip-stick alternating state and the frequency band-width where slipping phenomena occur within the selected frequency range.
In Figures 20-a to 20-d, four comparisons are shown between simulations and experiments. In detail, low excitation amplitude (0.2N in (a)), medium excitation amplitude (0.8N in (b) and 2N in (c)), and large excitation amplitudes (10N in (d)) are used. The separate contributions of the three harmonics are shown as well as the 0-peak response, calculated by applying the inverse Fourier transform to the solution in the frequency domain to obtain the time domain response and taking the half of the difference between the minimum and maximum response in one fundamental period. It is possible to see that, when low excitation amplitudes are used, the simulation tends to underestimate the effect of friction damping. As long as the excitation increases, the comparison improves.

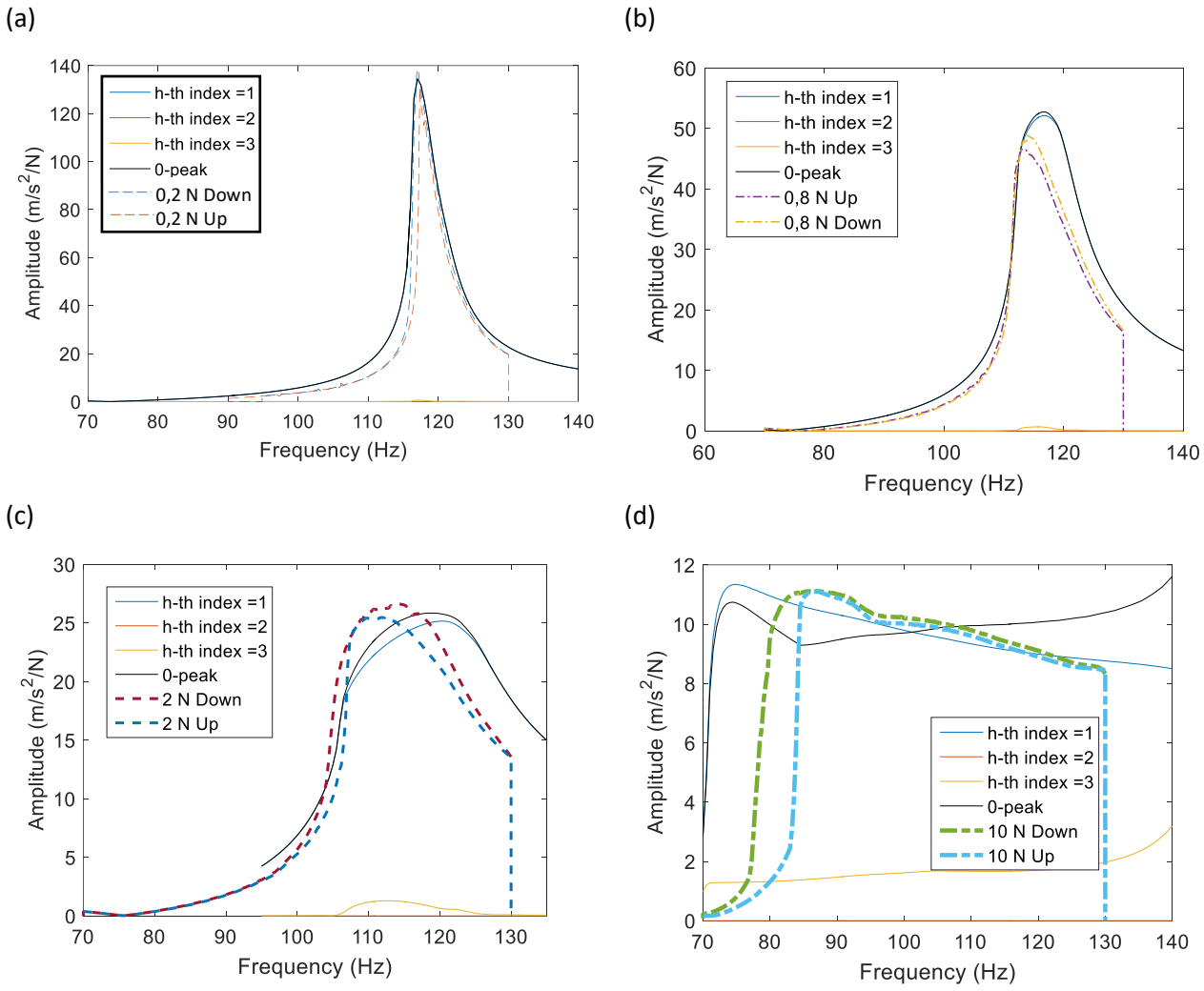

Fig.20 Numerical/experimental comparison for different excitation amplitudes: (a) 0.2N, (b) 0.8N, (c) 2N, (d) 10N. Numerical separate contributions for each h-th index and 0-peak (continuous lines) are plotted together with experimental responses (dashed lines).

It must be highlighted that the experimental responses for a low excitation amplitude like 0.2N are an average of multiple responses that give a noticeable dispersion. This is due to the difficulty to control such low values by the acquisition system.
Another interesting result comes from the comparison at large excitation loads (see Fig. 20 (d), 10 N excitation amplitude): the simulation shows that the third order harmonic response participates to the global response in a visible way by increasing the 0-peak response for a frequency range higher than 85 Hz, i.e., far from the resonance response determined by the fundamental frequency. On the contrary, the shape of the calculated first order harmonic is close to the measured response. This result reminds that the mathematical process to obtain the experimental FRF is actually a linearization of the dynamic response. The simplest operation that a software does in a digital data processing to calculate the FRF is simply the ratio of the spectrum of the response and the spectrum of the excitation force, frequency by frequency. Therefore, only the harmonic component associated to the fundamental frequency is used to obtain the FRF while the other components are filtered out.
The contact status is plotted in Fig. 21-22 in terms of separation, slipping and sticking status during one fundamental period of oscillation for the two resonant peaks of Fig.10a and d. The colormap indicates the amount of time in which the contact status remains within one fundamental period (scaled to 1). Only half of the contact surface is plotted, the symmetry plane is at Y = 0.2m . Some comments can be made by looking at the figures: a wide area is always in separation and this result does not depend on the excitation amplitude, in detail, only a circular area below the permanent magnet is in contact as in a receding contact. This result seems to be in contrast to what has been observed in [34] but it must be noted that the beams used in this test campaign are much more flexible than the assembly coupled by means of bolted joints in [34]. The slip state is mainly localized in correspondence of the outer boundary of the magnet, since it is a region where the normal preload is not large enough to cause sticking and at the same time no separation occurs. A limited number of contact elements are therefore actually dampening the structure for low excitation amplitudes. As long as the excitation force increases, the contact elements within the circular regions are subjected to an alternate stick/slip state. By looking at the circular shape, the amount of damping is larger when it occurs far from the central constraint located at y = 0.2 m.

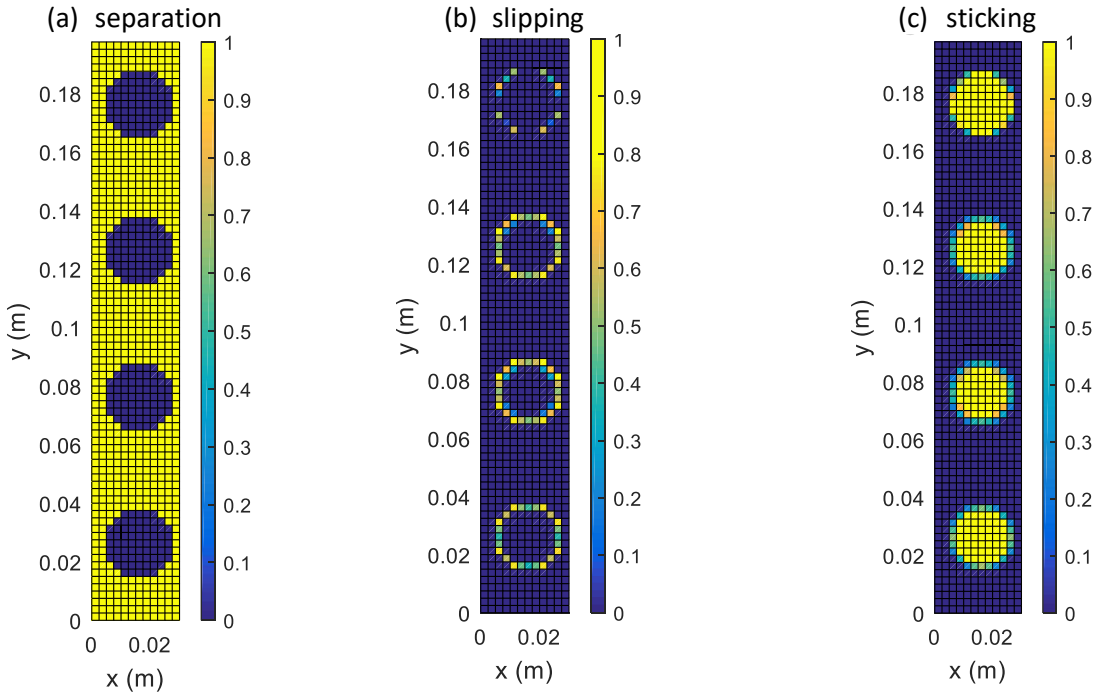

Fig.21 Separation (a), slipping (b) and sticking (c) for the peak response, excitation amplitude 0.2N. Colormaps indicate the time fraction of each contact status within one fundamental period (scaled to 1).

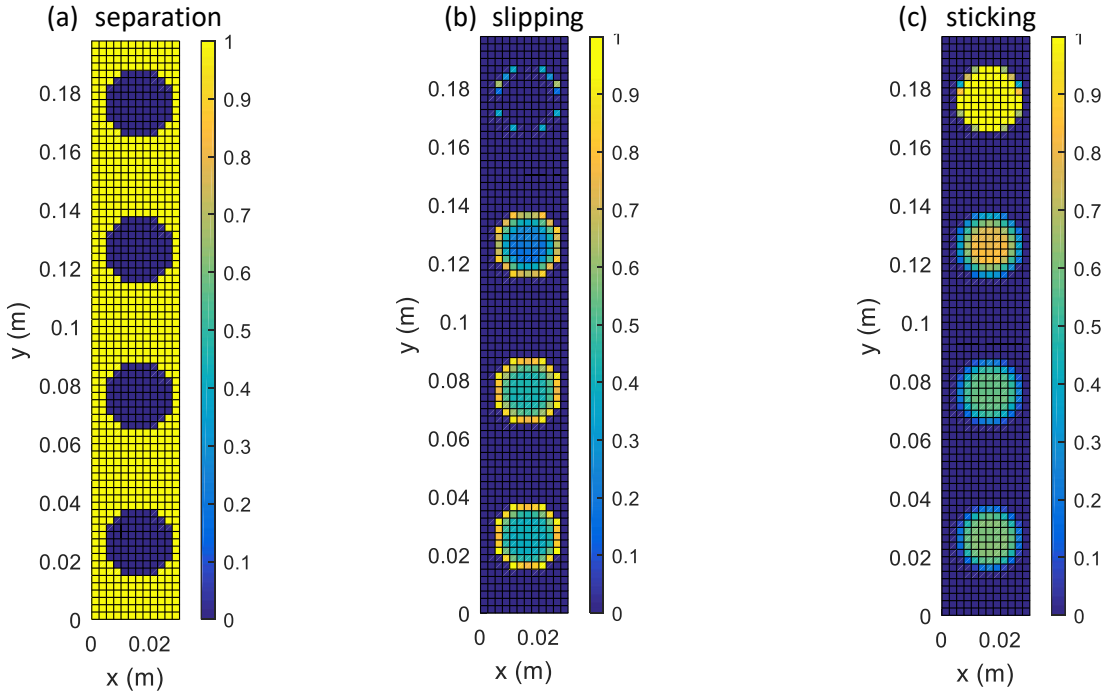

Fig.22 Separation (a), slipping (b) and sticking (c) for the peak response, excitation amplitude 10N. Colormaps indicate the time fraction of each contact status within one fundamental period (scaled to 1).

5 Conclusions

In this paper a reduction technique based on the Gram-Schmidt Interface method is applied to calculate the nonlinear forced response of a simple dynamic system made by two flexible beams coupled by means of permanent magnets and damped by a wide friction contact. The study aimed at producing friction damping due to large contact surfaces in order to highlight the convenience to use GSI mode shape instead of physical nodes at the interface in a full FE model. Contact elements based on penalty formulation and stick-slip-separation behavior are used and proved to be effective when used for large contact surfaces by comparing simulations with experiments.

Experimental test campaign is performed for validation purpose. The application of permanent magnets to couple the two beams prevented the presence of uncertainty due to bolted joints while keeping the receding contact. Nevertheless, the lack of holes led to an actual wide contact region that can still be considered wide with respect to the assembly.

The experimental/numerical comparison shows a general agreement of the measured FRF with the simulated ones in spite of a very fast computation with respect to the full FE transient analysis which led to unsatisfactory results. In detail, simulations performed with GSI reduction technique and Harmonic Balance Method showed that a small circular area around the permanent magnet is responsible for the friction damping (particularly for low excitation amplitudes), therefore dedicated and refined contact modeling is suggested to better simulate the localization of the friction contact in spite of a loss of a general approach involving all the nominal contact area.

The convenience of the GSI reduction technique will be better emphasized when multiple large contact interfaces are considered in a multi-component mechanical system. Despite the limited practical implications of the experimental setup in validating the methodology for engineering applications, it requires a simple hardware to collect a database of frictionally damped forced responses. Furthermore, this study has a valuable content from the educational point of view since it gave the possibility to students to graduate and enter for the first time to the world of friction nonlinearities. Acknowledgements go therefore to Massimo

Balvis, Mariacristina Caruso, Elisabetta Fogliasso, Claudio Gaglio, Gennaro Glionna, Luca Rossetti for participating with the authors in the development of this study.

Keywords:
Reduction technique; Large contacts; lap joint coupling; experimental validation; friction damping

References

[1] S. Bograd, P. Reuss, A. Schmidt, L. Gaul, M. Mayer, Modeling the dynamics of mechanical joints, Mechanical Systems and Signal Processing, 25 (2011), pp. 2801–2826, doi:10.1016/j.ymssp.2011.01.010.

[2] R.A. Ibrahim, C.L. Pettit, Uncertainties and dynamic problems of bolted joints and other fasteners, Journal of Sound and Vibration 279 (2005), pp. 857–936, doi:10.1016/j.jsv.2003.11.064.

[3] A. Mathis, N.N. Balaji, R. Kuether, A. Brink, M.R.W. Brake, D.D. Quinn, A Review of Damping Models for Structures with Mechanical Joints, ASME Applied Mechanics Reviews, Paper no. AMR-19-1056, doi:10.1115/1.4047707

[4] R. N. Coppolino, DOF Reduction Strategy for Large Order Finite Element Models, in Linking Models and Experiments, 2011, vol. 2, pp. 359–366

[5] Hughes, Patrick J., et al. Interface Reduction on Hurty/Craig-Bampton Substructures with Frictionless Contact, in Nonlinear Dynamics, Volume 1. Springer, Cham, 2019. 1-16.

[6] Firrone C. M., Battiato G., Epureanu B. I.: Modeling the Microslip in the Flange Joint and its Effect on the Dynamics of Multi-Stage Bladed Disks, Journal of Computational and Nonlinear Dynamics, January 2018, Vol. 13, DOI: 10.1115/1.4037796.

[7] Yang, B. D., Chu, M. L., & Menq, C. H. (1998). Stick–slip–separation analysis and non-linear stiffness and damping characterization of friction contacts having variable normal load. Journal of Sound and vibration, 210(4), 461-481.

[8] Christian Siewert, Lars Panning, Jorg Wallaschek, Christoph Richter, Multiharmonic forced response analysis of a turbine blading coupled by nonlinear contact forces, Proceedings of ASME Turbo Expo 2009: Power for Land, Sea and Air GT2009, June 8-12, 2009, Orlando, Florida, USA, GT2009-59201

[9] Petrov, E. P., & Ewins, D. J. (2006). Effects of damping and varying contact area at blade-disk joints in forced response analysis of bladed disk assemblies.

[10] S.M. Pourkiaee, S. Zucca, A reduced order model for nonlinear dynamics of mistuned bladed disks with shroud friction contacts, J. Eng. Gas Turbines Power 141 (1) (2019) 011031.

[11] Yuan, J., Salles, L., El Haddad, F., & Wong, C. (2020). An adaptive component mode synthesis method for dynamic analysis of jointed structure with contact friction interfaces. Computers & Structures, 229, 106177.

[12] Kuether, Robert J., Peter B. Coffin, and Adam R. Brink. "On Hurty/Craig-Bampton substructuring with interface reduction on contacting surfaces." International Design Engineering Technical Conferences and Computers and Information in Engineering Conference. Vol. 58226. American Society of Mechanical Engineers, 2017.

[13] Hughes, P., Scott, W. E., & Wu, W. (2017). Interface Reduction on Hurty/Craig-Bampton Substructures with Mechanical Joints (No. SAND2017-7824C). Sandia National Lab.(SNL-NM), Albuquerque, NM (United States).

[14] G. Battiato, C.M. Firrone, T.M. Berruti, B.I. Epureanu, Reduced order modeling for multistage bladed disks with friction contacts at the flange joint, J. Eng. Gas Turbines Power 140 (5) (2018) 052505.

[15] Singh, Aabhas, Matthew S. Allen, and Robert J. Kuether. "Substructure Interface Reduction with Iwan Elements to Capture Nonlinearity."

[16] Pichler, F., Witteveen, W., & Fischer, P. (2017). A complete strategy for efficient and accurate multibody dynamics of flexible structures with large lap joints considering contact and friction. Multibody System Dynamics, 40(4), 407-436.

[17] Géradin, Michel, and Daniel J. Rixen. "A 'nodeless' dual superelement formulation for structural and multibody dynamics application to reduction of contact problems." International Journal for Numerical Methods in Engineering 106.10 (2016): 773-798.

[18] Battiato, G., Firrone, C.M., Berruti, T.M., Epureanu, B.I.: Reduction and coupling of substructures via Gram–Schmidt Interface modes. Computer Methods in Applied Mechanics and Engineering, 336, 187-212.

[19] Battiato, G., Firrone, C.M., Reduced order modeling for forced response prediction of structures with large contact interfaces. Proceedings of ISMA Conference, Leuven, Belgium (2018).

[20] Battiato, G., and C. M. Firrone. "A modal based reduction technique for wide loose interfaces and application to a turbine stator." Mechanical Systems and Signal Processing 139 (2020): 106415.

[21] L. Gaul and J. Lenz, Stuttgart, Nonlinear dynamics of structures assembled by bolted joints, Acta Mechanica 125, 169-181 (1997).

[22] Jaime Esteban, Craig A. Rogers, Energy dissipation through joints: theory and experiments, Computers and Structures 75 (2000), pp. 347-359.

[23] Usik Lee, Dynamic characterization of the joints in a beam structure by using spectral element method, Shock and Vibration 8 (2001) 357–366.

[24] Y. Songa, C.J. Hartwigsenb, D.M. McFarlanda, A.F. Vakakisb, L.A. Bergman, Simulation of dynamics of beam structures with bolted joints using adjusted Iwan beam elements, Journal of Sound and Vibration 273 (2004), pp. 249–276, doi: 10.1016/S0022-460X(03)00499-1.

[25] J. Gross, J. Armand, R.M. Lacayo, P. Reuss, L. Salles, C.W. Schwingshackl, M.R.W. Brake, R.J. Kuether, A Numerical Round Robin for the Prediction of the Dynamics of Jointed Structures, Dynamics of Coupled Structures, Volume 4. Conference Proceedings of the Society for Experimental Mechanics Series. Springer, Cham, https://doi.org/10.1007/978-3-319-29763-7_20

[26] Gruber, F.M., Rixen, D.J., Evaluation of Substructure Reduction Techniques with Fixed and Free Interfaces. Journal of Mechanical Engineering 62(2016)7-8, 452-462, DOI:10.5545/sv-jme.2016.3735.

[27] Castanier M. P., Yung-Chang T., and Pierre C., Characteristic constraint modes for component mode synthesis. AIAA journal 39.6 (2001): 1182-1187.

[28] Gilbert Strang. Introduction to linear algebra. Wellesley, MA: Wellesley-Cambridge Press, 1993.

[29] N.N. Balaji, W. Chen, M.R.W. Brake, Traction-based multi-scale nonlinear dynamic modeling of bolted joints: Formulation, application, and trends in micro-scale interface evolution, Mechanical Systems and Signal Processing 139 (2020), doi: 10.1016/j.ymssp.2020.106615

[30] J.P. Lopes, D.A. Hills, The axisymmetric frictional receding contact of a layer pressed against a half-space by a point force, International Journal of Solids and Structures 171 (2019), pp. 47–53, doi.org/10.1016/j.ijsolstr.2019.05.007.

[31] Schwingshackl, C., Di Maio, D., Sever, I.A., and Green, J.S., Modeling and Validation of the Nonlinear Dynamic Behavior of Bolted Flange Joints, J.E. Gas Turbines Power, Jul 2013, Vol 135, Issue 12

[32] R. M. Lacayo, L. Pesaresi, D. Fochler, J. Gross, J. Armand, L. Salles, M.R.W. Brake, C.W. Schwingshackl, A comparison of numerical approaches for predicting the dynamics of a beamwith a lap joint.

[33] Willner, K., Identification of contact parameters for dry friction joints. Proceedings of ISMA Conference, Leuven, Belgium (2018).

[34] Brake M.R.W., Stark J.G., Smith S.A., Lancereau D.P.T., Jerome T.W., Dossogne T. (2017) In Situ Measurements of Contact Pressure for Jointed Interfaces During Dynamic Loading Experiments. In: Allen M., Mayes R., Rixen D. (eds) Dynamics of Coupled Structures, Volume 4. Conference Proceedings of the Society for Experimental Mechanics Series. Springer, Cham